© 2016 IJSRSET | Volume 2 | Issue 2 | Print ISSN : 2395-1990 | Online ISSN : 2394-4099
Themed Section: Engineering and Technology

Effect of Alloying Elements on Electrochemical Corrosion Behavior, Microstructure, Wettability and Thermal Performance of Bismuth-Tin Based Alloys

Abu Bakr El-Bediwi[1], S. Bader[1], Fathia Khalifa[1, 2]

[1]Metal Physics Lab., Physics Department, Faculty of Science, Mansoura University, Egypt
[1, 2]Sirte University, Sirte, Libya

ABSTRACT

Microstructure, wettability behavior, corrosion parameters, thermal properties of quaternary bismuth- tin based alloy have been investigated using different experimental techniques. Induced lattice microstrain of $Bi_{60}Sn_{40}$ alloy increased after adding Sb-Zn or Sb-Ag or Al-Cd or Al-Cu. Contact angle of $Bi_{60}Sn_{40}$ alloy increased after adding Sb-Zn or Sb-Ag or Al-Cd or Al-Cu. A significant change (28%) occurred in contact angle of $Bi_{60}Sn_{40}$ alloy after adding Al-Cd. Corrosion rate of $Bi_{60}Sn_{40}$ alloy decreased after adding Sb-Zn or Sb-Ag but it increased after adding Al-Cd or Al-Cu. The melting temperature of $Bi_{60}Sn_{40}$ alloy varied after adding alloying elements. The $Bi_{50}Sn_{40}Al_5Cd_5$ alloy has the lowest melting temperature. Some properties of $Bi_{60}Sn_{40}$ alloy improved after adding Sb-Zn or Sb-Ag elements which make them useful for different industrial applications.
Keywords: Corrosion Behavior, Wettability, Microstructure, Melting Point, Thermal Performance, Pasty Range, Bismuth-Tin Alloys

I. INTRODUCTION

Bismuth is used in alloys to lower the melting point as in industry applications such as thermal switches. Much research was done for studying microstructure, electrical, mechanical and thermal properties of bismuth- lead/ bismuth-tin eutectic alloys, bismuth- lead- tin, bismuth- lead- tin- cadmium, tin- antimony with other elements additions [1-11]. The microstructure and microhardness of rapidly solidified foils of the Sn-58 wt. % Bi alloy was studied [12]. The Sn-Bi eutectic alloy nanoparticle consisted of the tetragonal phase of tin and the rehombohedral phase of bismuth [13]. The Bi-Sn eutectic alloy has a good soldering property such as low melting point, mechanical properties, adequate wettability and cost [14]. Splat quenching caused a metastable shift of the solubility limit in Sn-Bi alloys containing 15, 20 and 25 % bismuth [15]. The ductility of the binary Bi-Sn eutectic solders has significantly improved by adding small amount of Ag [16]. The phase formation during rapid solidification of the undercooled droplets Bi-Sn system at ambient pressure and of the thermal behavior of droplet samples under hydrostatic pressure conditions in an attempt to identify the structure and the operative solidification kinetics were studied [17]. The microstructural development of eutectic alloys Bi-Sn and In-Sn during high temperature deformation was studied and reported [18]. The aim of our research was to study the effect of quaternary alloying elements on microstructure, electrochemical corrosion behavior and soldering properties of bismuth-tin alloy.

II. METHODS AND MATERIAL

High purity (more than 99.5 %) bismuth, tin, antimony, zinc, silver, aluminum, cadmium and copper were melted in a muffle furnace to use in the production ingots from $Bi_{60}Sn_{40}$, $Bi_{50}Sn_{40}Sb_7Zn_3$, $Bi_{50}Sn_{40}Sb_7Ag_3$, $Bi_{50}Sn_{40}Al_5Cd_5$ and $Bi_{50}Sn_{40}Al_8Cu_2$ alloys. The resulting ingots were turned and re-melted four times to increase the homogeneity. Long ribbons of ~ 3 mm width and

~90 µm thickness were prepared by melt spinning technique. The surface velocity of the roller was 31.4 m/s giving a cooling rate of ~3.7 × 10^5 K/s. The samples then cut into convenient shape for the measurements using double knife cuter. Microstructure of used samples was performed using scanning electron microscope (JEOL JSM-6510LV, Japan) and Shimadzu X–ray Diffractometer (Dx–30, Japan) of Cu–Kα radiation with λ=1.54056Å at 45 kV and 35 mA and Ni–filter in the angular range 2θ ranging from 0 to 100° in continuous mode with a scan speed 5 deg/min. Thermal analysis were obtained using SDT Q600 (V20.9 Build 20) instrument made in U. S. A with heating rate 10 k/min in the temperature range from 50-400 °C. All the samples have the same mass, which is 2 mg. The polarization studies were performed using Gamry Potentiostat/Galvanostat with a Gamry framework system based on ESA 300.

III. RESULTS AND DISCUSSION

A. Microstructure

Figure 1a shows x-ray diffraction patterns of $Bi_{60}Sn_{40}$ alloy which have lines corresponding to hexagonal bismuth phase and tetragonal tin phase. Stared base line at ~ 240 counts and the range of random atoms distribution (amorphousity area) stared from 0 to 35°. X-ray diffraction patterns of $Bi_{50}Sn_{40}Sb_7Zn_3$ alloy which have lines corresponding to hexagonal bismuth phase and tetragonal tin phase as shown in Figure 1b. That meant that, antimony and zinc atoms dissolved in matrix alloy formed a solid solution. Adding 7% antimony and 3% zinc improve crystallinty which indicated by peak intensity and decreased amorphous region (0- 28°) with formed a small phases in it\ or undetected phases. X-ray diffraction patterns of $Bi_{50}Sn_{40}Sb_7Ag_3$ alloy which have lines corresponding to hexagonal bismuth phase and tetragonal tin phase as shown in Figure 1c. That meant that, antimony and silver atoms dissolved in matrix alloy. Adding 7% antimony and 3% silver caused little enhanced in $Bi_{60}Sn_{40}$ crystallinty. X-ray diffraction patterns of $Bi_{50}Sn_{40}Al_5Cd_5$ alloy which have lines corresponding to hexagonal bismuth phase and tetragonal tin phase as shown in Figure 1d. That meant that, aluminum and cadmium atoms dissolved in matrix alloy. Adding 5% aluminum and 5% cadmium enhance $Bi_{60}Sn_{40}$ crystallinty. X-ray diffraction patterns of $Bi_{50}Sn_{40}Al_8Cu_2$ alloy which have lines corresponding to hexagonal bismuth phase, tetragonal tin phase and CuSn intermetallic phase as shown in Figure 1e. That meant that, aluminum and cadmium atoms dissolved in matrix alloy. Adding 8% aluminum and 2% copper improve $Bi_{60}Sn_{40}$ crystallinty and decreased amorphous region. The analysis of x-ray diffraction patterns, (peak intensity, peak broadness, peak position, area under peaks, phases and Miller indices), is shown in Table 1 (a, b, c, d and e). The estimated crystal size is given by Scherer equation [19] and then listed in Table 1f.

Lattice microstrain will be related to both diffraction lines broadening as well as line shift compared with the initial state. From the relation between full widths half maximum (β) and 4tanθ [20, 21] as shown in Figure 1f, the induced internal lattice microstrain of used alloys was determined and then listed in Table 1g. Lattice microstrain of $Bi_{60}Sn_{40}$ alloy increased after adding quaternary elements, Sb-Zn or Sb- Ag or Al- Cd or Al-Cu, that is because Sb, Ag or Sb, Zn or Al, Cd or Al, Cu atoms dissolved in matrix alloy effected on its structure.

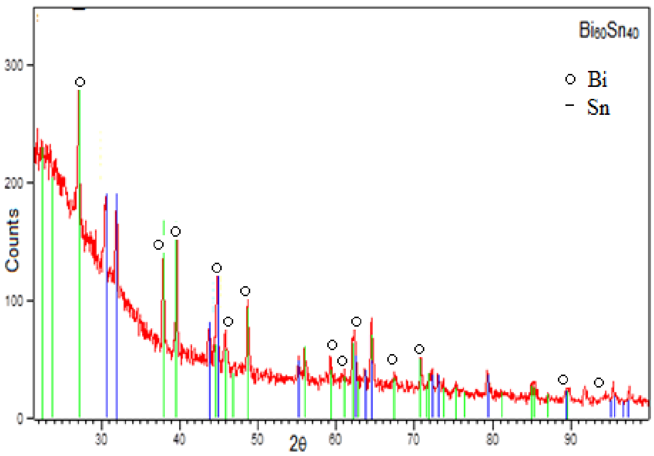

Figure 1a:-x-ray diffraction patterns of $Bi_{60}Sn_{40}$ alloy

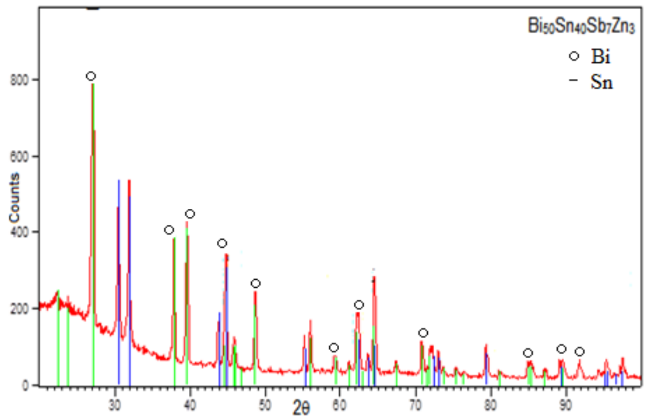

Figure 1b:-x-ray diffraction patterns of $Bi_{50}Sn_{40}Sb_7Zn_3$ alloy

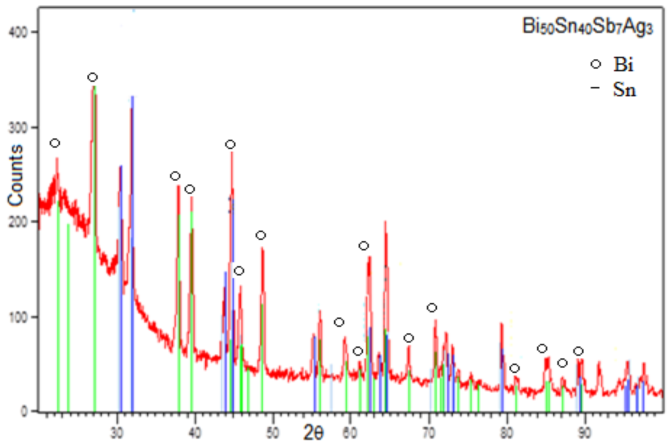

Figure 1c:-x-ray diffraction patterns of $Bi_{50}Sn_{40}Sb_7Ag_3$ alloy

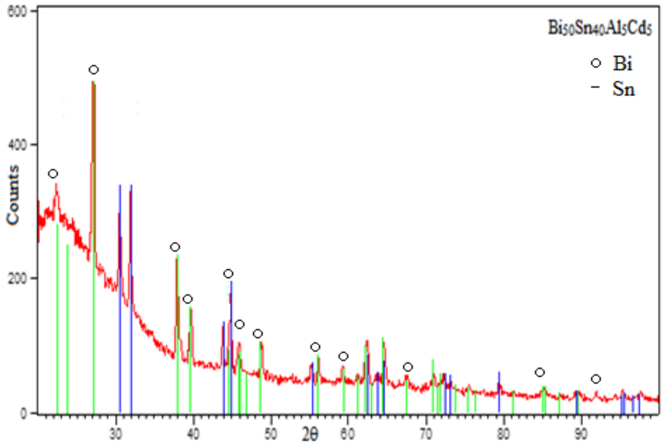

Figure 1d:-x-ray diffraction patterns of $Bi_{50}Sn_{40}Al_5Cd_5$ alloy

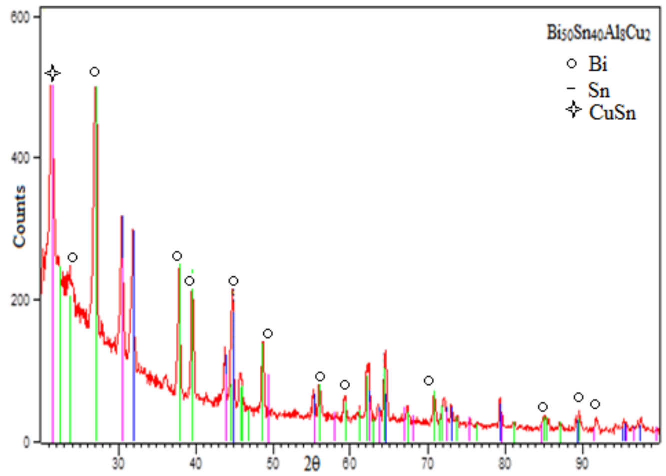

Figure 1e:-x-ray diffraction patterns of $Bi_{50}Sn_{40}Al_8Cu_2$ alloy

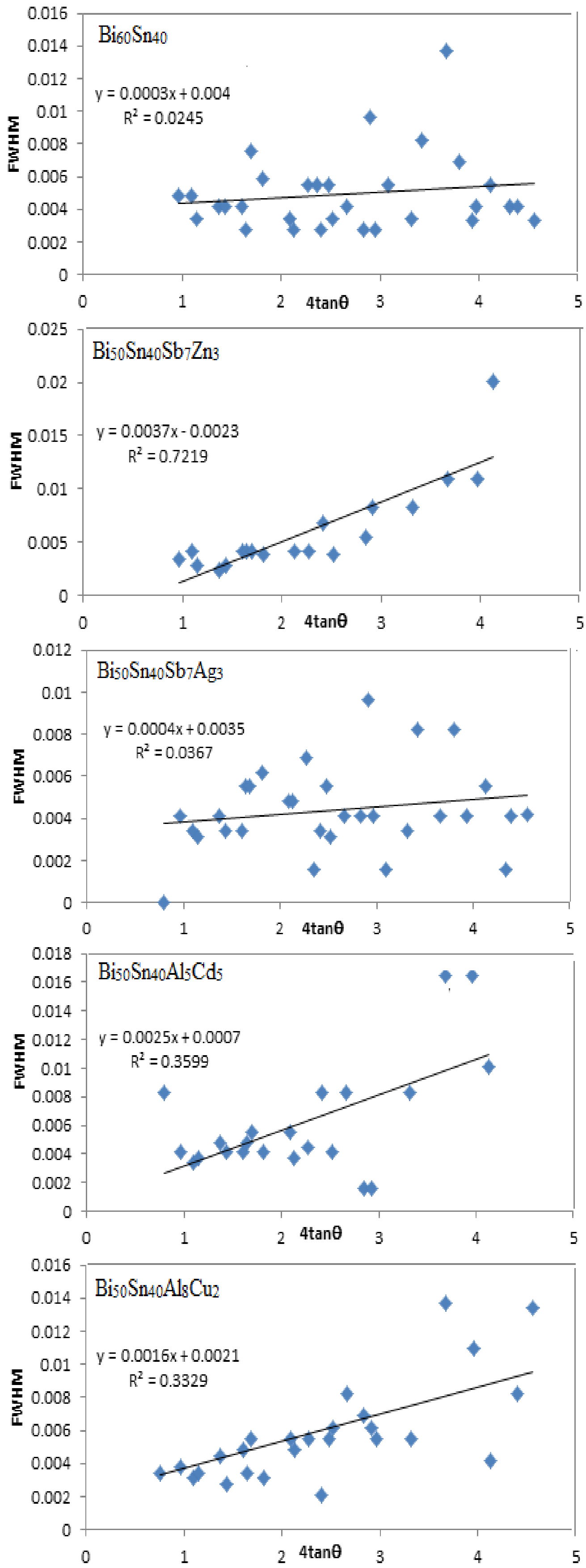

Figure 1f :- FWHM versus 4tanθ for used alloys

Table 1a:- x-ray diffraction analysis of $Bi_{60}Sn_{40}$ alloy

2Θ	d A°	Int.%	FHWM	Area	Phase	hkl
27.1398	3.28574	100	0.2755	225.35	Bi	012
30.5471	2.92656	44.63	0.2755	100.58	Sn	200
31.9955	2.7973	46.86	0.1968	75.42	Sn	101
37.9723	2.36964	35.47	0.2362	68.51	Bi	104
39.6627	2.27246	44.17	0.2362	85.32	Bi	110
43.7598	2.06873	14.05	0.2362	27.13	Sn	220
44.8202	2.02222	37.6	0.1574	48.42	Bi	211
45.8654	1.97854	9.25	0.433	32.77	Bi	113
48.7203	1.86907	25.17	0.3346	68.86	Bi	202
55.2121	1.66369	11.36	0.1968	18.28	Sn	301
55.9846	1.64255	16.26	0.1574	20.93	Sn	301
59.2961	1.55848	5.38	0.3149	13.86	Bi	107
61.1275	1.51611	2.68	0.3149	6.9	Bi	205
62.1275	1.49409	17.16	0.1574	22.09	Bi	116
63.6578	1.46181	5.46	0.3149	14.06	Sn	400
64.5163	1.44442	30.55	0.1968	49.17	Sn	321
67.4003	1.38946	4.04	0.2362	7.8	Bi	018
70.7542	1.3316	11.12	0.1574	14.32	Bi	214
71.9365	1.3126	8.03	0.551	36.21	Sn	420
72.9657	1.2966	7.1	0.1574	9.15	Sn	411
75.3333	1.26163	2.82	0.3149	7.27	Bi	125
79.352	1.20752	10.31	0.1968	16.6	Sn	312
81.2294	1.18429	1.24	0.4723	4.8	Bi	208
85.1387	1.13963	3.76	0.7872	24.21	Bi	119
87.0591	1.11936	2.86	0.3936	9.2	Bi	217
89.1342	1.09769	5.68	0.192	12.09	Bi	306
89.5669	1.09441	5.93	0.2362	11.45	Bi	306
91.7129	1.07433	5.18	0.3149	13.33	Bi	312
94.3053	1.05151	2.04	0.2362	3.94	Bi	128
95.3808	1.04249	5.18	0.2362	10	Sn	332
97.5634	1.02406	5.94	0.192	12.61	Sn	521

Table 1b:- x-ray diffraction analysis of $Bi_{50}Sn_{40}Sb_7Zn_3$ alloy

2Θ	d A°	Int.%	FHWM	Area	Phase	hkl
27.1339	3.28644	100	0.1968	36.27	Bi	012
30.546	2.92666	35.26	0.2362	15.34	Sn	200
31.9344	2.80252	39.13	0.1574	11.35	Sn	101
37.9547	2.3707	50.81	0.1378	12.9	Bi	104
39.6161	2.27502	54.19	0.1574	15.72	Bi	110
43.7766	2.06797	16.01	0.2362	6.97	Sn	220
44.7808	2.0239	43.91	0.2362	19.11	Sn	220
45.8833	1.97781	19.77	0.2362	8.61	Bi	113
48.7704	1.86727	35.89	0.2165	14.32	Bi	202
56.0277	1.64139	15.43	0.2362	6.72	Sn	301
59.2999	1.5584	11.81	0.2362	5.14	Bi	107
62.2443	1.49156	20.9	0.3936	15.16	Bi	116
64.5636	1.44347	29.61	0.2165	11.81	Sn	321
70.8319	1.33033	14.42	0.3149	8.37	Bi	214
72.1252	1.30963	6.94	0.4723	6.04	Sn	411
79.4731	1.20599	6.88	0.4723	5.99	Sn	312
85.1493	1.13951	4.86	0.6298	5.64	Bi	119
89.6991	1.09314	6.77	0.6298	7.86	Bi	306
91.866	1.07205	3.94	1.152	11.29	Bi	312

Table 1c:- x-ray diffraction analysis of $Bi_{50}Sn_{40}Sb_7Ag_3$ alloy

2Θ	d A°	Int.%	FHWM	Area	Phase	hkl
22.41	3.96736	68.52	0.001	0.12	Bi	003
27.1674	3.28246	100	0.2362	60.63	Bi	012
30.5933	2.92225	45.13	0.1968	22.8	Sn	200
31.9732	2.79921	75.41	0.1771	34.29	Sn	101
37.9076	2.37353	67.02	0.2362	40.63	Bi	104
39.6466	2.27334	62.26	0.1968	31.45	Bi	110
43.7368	2.06976	30.46	0.1968	15.39	Sn	220
44.763	2.02467	85.84	0.3149	69.39	Bi	211
45.8189	1.98044	31.22	0.3149	25.24	Bi	113
48.7219	1.86901	48.81	0.3542	44.39	Bi	202
55.2854	1.66166	17.26	0.2755	12.21	Sn	301
55.9801	1.64267	26.06	0.2755	18.43	Sn	301
59.2153	1.56042	15.86	0.3936	16.02	Bi	107
61.01	1.51875	3.07	0.09	0.72	Bi	205
62.4077	1.48805	46.11	0.1968	23.29	Bi	116
63.6117	1.46276	9.29	0.3149	7.51	Sn	400
64.4464	1.44582	62.22	0.1771	28.29	Sn	321
67.3895	1.38966	13.73	0.2362	8.32	Bi	018
70.7525	1.33163	23.7	0.2362	14.37	Bi	214
72.173	1.30888	19.23	0.551	27.2	Sn	411
73.0033	1.29603	14.57	0.2362	8.84	Sn	411
75.47	1.25968	4.23	0.09	0.99	Bi	125
79.3064	1.2081	25.84	0.1968	13.05	Sn	312
81.2279	1.18431	5.45	0.4723	6.61	Bi	208
84.9137	1.14207	14.02	0.2362	8.5	Bi	119
87.1714	1.11821	5.45	0.4723	6.6	Bi	217
89.1172	1.09877	13.88	0.2362	8.42	Bi	306
91.7556	1.07394	12.28	0.3149	9.92	Bi	312
94.59	1.0491	3.84	0.09	0.9	Sn	332
95.3959	1.04236	11.77	0.2362	7.14	Sn	332
97.5548	1.02412	11.68	0.24	9.72	Sn	521

Table 1d: - x-ray diffraction analysis of $Bi_{50}Sn_{40}Al_5Cd_5$ alloy

2Θ	d A°	Int.%	FHWM	Area	Phase	hkl
22.3795	3.9727	20.49	0.4723	37.01	Bi	003
27.1793	3.28105	100	0.2362	90.3	Bi	012
30.5751	2.92395	39.2	0.1968	29.5	Sn	200
31.9142	2.80425	47.07	0.2165	38.96	Sn	101
37.8705	2.37578	35.63	0.2755	37.53	Bi	104
39.6137	2.27516	21.91	0.2362	19.78	Bi	110
43.7945	2.06717	16.27	0.2362	14.69	Sn	220

44.8698	2.0201	29.3	0.2755	30.87	Bi	211
45.8473	1.97928	12.26	0.3149	14.77	Bi	113
48.7795	1.86694	13.04	0.2362	11.78	Bi	202
55.2365	1.66301	8.19	0.3149	9.87	Sn	301
56.0549	1.64066	10.54	0.2165	8.72	Bi	024
59.2589	1.55938	6.85	0.2558	6.7	Bi	107
62.3788	1.48867	15.9	0.4723	28.71	Sn	112
64.5026	1.44469	15.95	0.2362	14.4	Sn	321
67.4439	1.38867	4.83	0.4723	8.73	Bi	018
70.81	1.33069	4.9	0.09	1.71	Bi	214
72.35	1.30611	2.84	0.09	0.99	Sn	411
79.4057	1.20684	3.73	0.4723	6.74	Sn	312
85.2375	1.13856	2.72	0.9446	9.83	Bi	119
89.5286	1.09478	2.85	0.9446	10.29	Bi	306
91.8855	1.07188	3.43	0.576	10.22	Bi	312

Table 1e: - x-ray diffraction analysis of $Bi_{50}Sn_{40}Al_8Cu_2$ alloy

2Ө	d A°	Int.%	FHWM	Area	phase	hkl
21.2911	4.17325	67.82	0.1968	59.04	CuSn	
23.8654	3.72861	8.37	0.6298	23.32	Bi	101
27.163	3.28299	100	0.2165	95.76	Bi	012
30.6045	2.92121	43.25	0.1771	33.88	Sn	200
31.9551	2.80076	42.86	0.1968	37.31	Sn	101
37.8122	2.3793	37.7	0.2558	42.66	Bi	104
39.6386	2.27378	37.68	0.1574	26.24	Bi	110
43.7676	2.06838	18.02	0.2755	21.96	Sn	220
44.7946	2.02332	37.86	0.1968	32.96	Bi	211
45.651	1.98733	8.83	0.3149	12.3	Bi	113
48.7426	1.86827	22.81	0.1771	17.87	Bi	202
55.211	1.66372	7.39	0.3149	10.29	Sn	301
56.006	1.64198	10.83	0.2755	13.2	Bi	024
59.253	1.55952	7.07	0.3149	9.84	Bi	107
62.099	1.49471	16.43	0.1181	8.58	Sn	112
63.5925	1.46315	4.76	0.3149	6.63	Sn	400
64.4889	1.44497	21.57	0.3542	33.8	Sn	321
67.4061	1.38935	4.12	0.4723	8.61	Bi	018
70.7828	1.33113	8.24	0.3936	14.34	Bi	214
72.1503	1.30923	7.71	0.3542	12.08	Sn	411
73.0073	1.29597	5.04	0.3149	7.01	Sn	411
79.3299	1.2078	7.66	0.3149	10.67	Sn	312
85.1251	1.13977	3.63	0.7872	12.63	Bi	119
89.447	1.09557	3.59	0.6298	10.01	Bi	306
91.7617	1.07389	4.92	0.2362	5.14	Bi	312
95.4735	1.04172	2.81	0.4723	5.86	Sn	332
97.4781	1.02472	3	0.768	13.76	Sn	521

Table 1f:-crystal size of Bi and Sn in used alloys

Alloys	(Bi) τ A°	(Sn) τ A°
$Bi_{60}Sn_{40}$	372.55	445.04
$Bi_{50}Sn_{40}Sb_7Zn_3$	337.28	300.9
$Bi_{50}Sn_{40}Sb_7Ag_3$	490.63	478.75
$Bi_{50}Sn_{40}Al_5Cd_5$	330.3	416.96
$Bi_{50}Sn_{40}Al_8Cu_2$	317.01	346.12

Table (1g):-lattice microstrain of used alloys

Alloys	Lattice microstrain $x\ 10^{-3}$
$Bi_{60}Sn_{40}$	0.3
$Bi_{50}Sn_{40}Sb_7Zn_3$	3.7
$Bi_{50}Sn_{40}Sb_7Ag_3$	0.4
$Bi_{50}Sn_{40}Al_5Cd_5$	2.5
$Bi_{50}Sn_{40}Al_8Cu_2$	1.6

Scanning Electron Micrographs Analysis

Scanning electron micrograph of $Bi_{60}Sn_{40}$ alloy, Figure 2a, shows the bismuth grain is majority as white color with different size, shape and orientations with large grain of tin as minority black color. Also scanning electron micrograph of $Bi_{50}Sn_{40}Sb_7Zn_3$ alloy, Figure 2b, shows the bismuth grain as majority white color with different size, shape and orientations with tin grains as minority black color. That is mean; adding antimony and zinc to $Bi_{60}Sn_{40}$ alloy caused a refinement grain size with increased homogeneity of it. Also small grain appeared as bright white color. Scanning electron micrograph of $Bi_{50}Sn_{40}Sb_7Ag_3$ alloy given in Figure 2c shows that, bismuth grain as majority white color with different size, shape and orientations with tin grains as minority black color. Adding antimony and silver to $Bi_{60}Sn_{40}$ alloy caused refinement to grain size with increased homogeneity of it. Many grains appeared as bright white color. Also very smooth dendrite from bright white color grains appeared. Scanning electron micrograph of $Bi_{50}Sn_{40}Al_5Cd_5$ alloy given in Figure 2d shows that, white color bismuth grain as lamellar structure (texture) with different size, shape and orientations with black color tin grains as dendrite structure. Adding aluminum and cadmium to $Bi_{60}Sn_{40}$ alloy caused more homogeneity of both phases.

Scanning electron micrograph of $Bi_{50}Sn_{40}Al_8Cu_2$ alloy, Figure 2e, shows the white color bismuth grains with different size, shape and orientations and black color tin grains. Also bright white color grains are disturbed in matrix alloy. Adding aluminum and copper to $Bi_{60}Sn_{40}$ alloy caused more homogeneity of both phases.

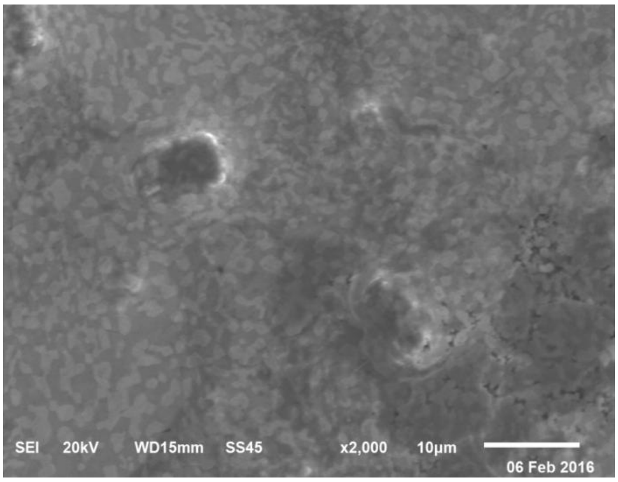

Figure 2a:-SEM of $Bi_{60}Sn_{40}$ alloy

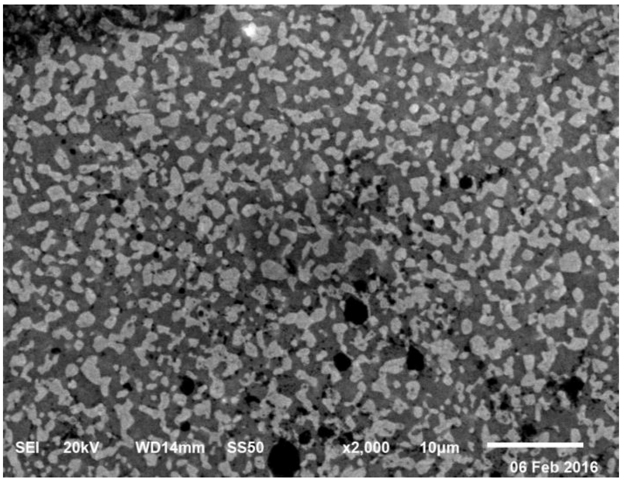

Figure 2b:- SEM of $Bi_{50}Sn_{40}Sb_7Zn_3$ alloy

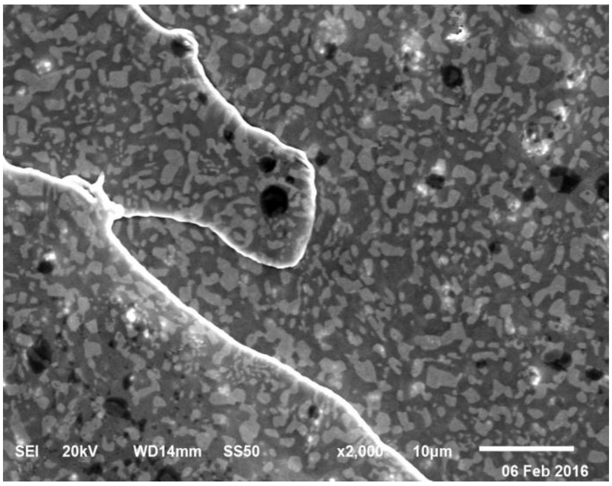

Figure 2c:- SEM of $Bi_{50}Sn_{40}Sb_7Ag_3$ alloy

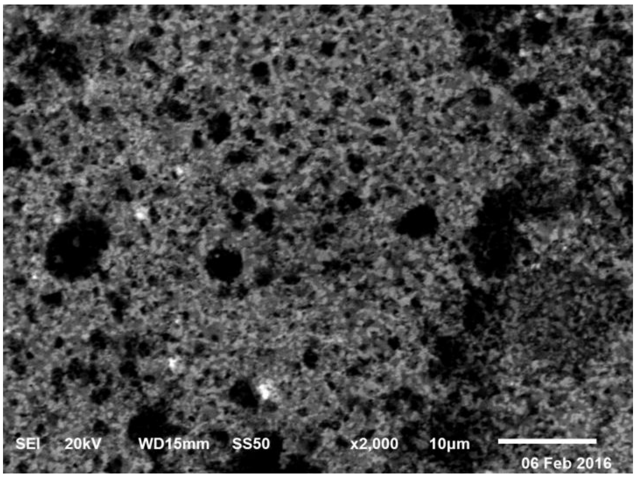

Figure 2d:- SEM of $Bi_{50}Sn_{40}Al_5Cd_5$ alloy

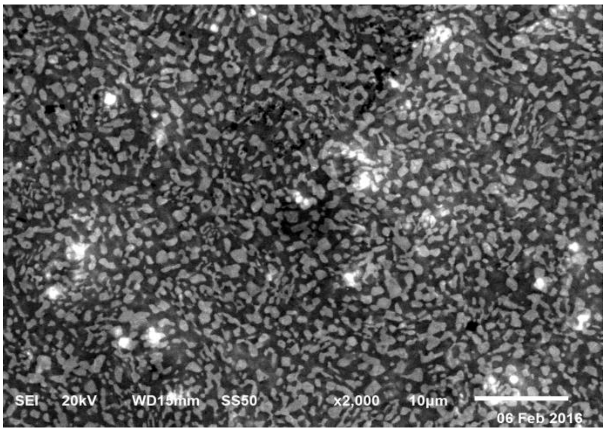

Figure 2e:- SEM of $Bi_{50}Sn_{40}Al_8Cu_2$ alloy

B. Wetting Behavior

Wetting is the ability of a liquid to maintain contact with a solid surface, resulting from intermolecular interactions when the two are brought together. The contact angle is determined by the resultant between adhesive and cohesive forces. As the tendency of a drop to spread out over a flat, solid surface increases, the contact angle decreases. Thus, the contact angle provides an inverse measure of wettability. The spreading of $Bi_{60}Sn_{40}$, $Bi_{50}Sn_{40}Sb_{7}Zn_{3}$, $Bi_{50}Sn_{40}Sb_{7}Ag_{3}$, $Bi_{50}Sn_{40}Al_{5}Cd_{5}$ and $Bi_{50}Sn_{40}Al_{8}Cu_{2}$ molten alloys on copper surface in air is shown in Figure 3. The measured contact angles of used alloys listed in Table 2. Contact angle of $Bi_{60}Sn_{40}$ alloy increased after adding Sb-Zn or Sb-Ag or Al-Cd or Al-Cu and a significant increased (28%) occurred after adding Al-Cd.

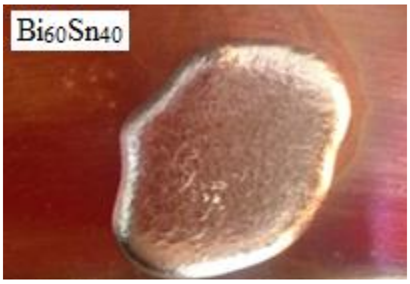

Figure 3:-spreading of used alloys on copper in air

Table 2:-measured contact angles of used alloys on copper in air

Alloys	Contact angle°
$Bi_{60}Sn_{40}$	48.75
$Bi_{50}Sn_{40}Sb_{7}Zn_{3}$	57.75
$Bi_{50}Sn_{40}Sb_{7}Ag_{3}$	57.5
$Bi_{50}Sn_{40}Al_{5}Cd_{5}$	62.5
$Bi_{50}Sn_{40}Al_{8}Cu_{2}$	56.25

C. Thermal performance

Melting temperature is very important for industrial and medicine applications. Thermo-graphs of $Bi_{60}Sn_{40}$, $Bi_{50}Sn_{40}Sb_{7}Zn_{3}$, $Bi_{50}Sn_{40}Sb_{7}Ag_{3}$, $Bi_{50}Sn_{40}Al_{5}Cd_{5}$ and $Bi_{50}Sn_{40}Al_{8}Cu_{2}$ alloys are shown in Figure 4. The melting point of used alloys is listed in Table (3). The melting temperature of $Bi_{60}Sn_{40}$ alloy varied after adding alloying elements. The $Bi_{50}Sn_{40}Al_{5}Cd_{5}$ alloy has lowest melting temperature.

The pasty range is the difference between solidus and liquidus points. The pasty range of $Bi_{60}Sn_{40}$, $Bi_{50}Sn_{40}Sb_{7}Zn_{3}$, $Bi_{50}Sn_{40}Sb_{7}Ag_{3}$, $Bi_{50}Sn_{40}Al_{5}Cd_{5}$ and $Bi_{50}Sn_{40}Al_{8}Cu_{2}$ alloys are listed in Table 3. The $Bi_{50}Sn_{40}Al_{8}Cu_{2}$ alloy has low pasty range value.

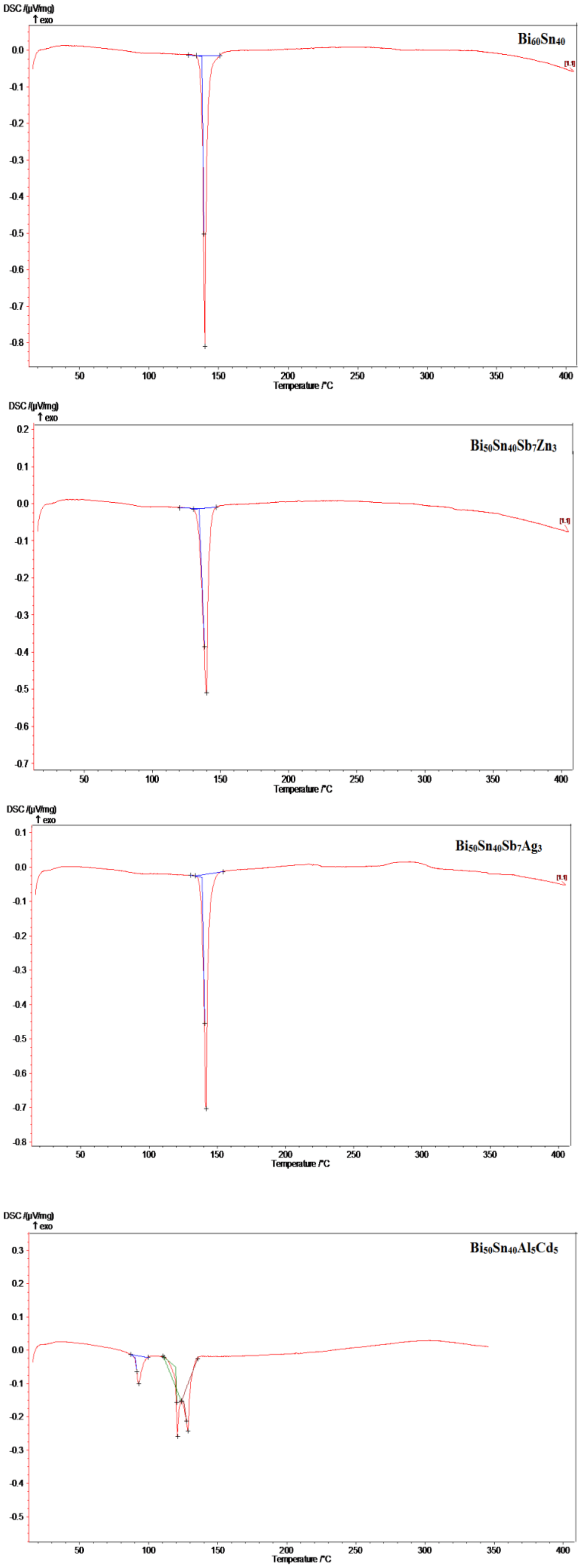

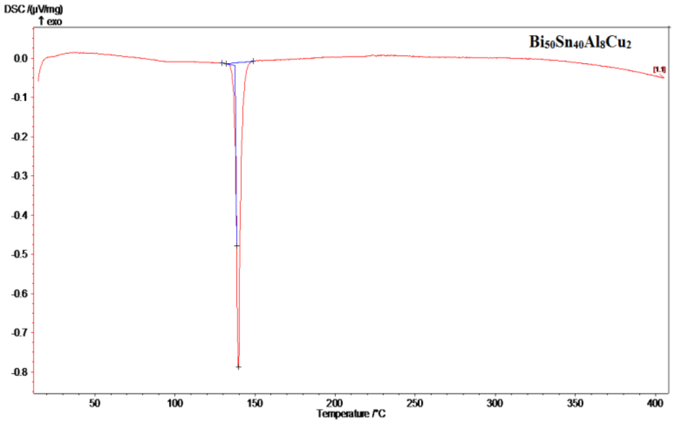

Figure 4:- DSC thermographs of used alloys

Table 3:- Melting Point And Pasty Range Of Used Alloys

Alloys	Melting point °C	Pasty range °C
$Bi_{60}Sn_{40}$	**140.3**	**1.3**
$Bi_{50}Sn_{40}Sb_7Zn_3$	**139.8**	**4**
$Bi_{50}Sn_{40}Sb_7Ag_3$	**142**	**1.5**
$Bi_{50}Sn_{40}Al_5Cd_5$	**128.4**	**-**
$Bi_{50}Sn_{40}Al_8Cu_2$	**139.7**	**1.2**

D. Electrochemical corrosion behavior

Electrochemical polarization curves of $Bi_{60}Sn_{40}$, $Bi_{50}Sn_{40}Sb_7Zn_3$, $Bi_{50}Sn_{40}Sb_7Ag_3$, $Bi_{50}Sn_{40}Al_5Cd_5$ and $Bi_{50}Sn_{40}Al_8Cu_2$ alloys in 0.5M HCl are shown in Figure 5. From this figure, the corrosion potential of used alloys exhibited a negative potential. Also the cathodic and the anodic polarization curves showed similar corrosion trends. The corrosion potential (E_{Corr}), corrosion current (I_{Corr}) and corrosion rate (C.R) of $Bi_{60}Sn_{40}$, $Bi_{50}Sn_{40}Sb_7Zn_3$, $Bi_{50}Sn_{40}Sb_7Ag_3$, $Bi_{50}Sn_{40}Al_5Cd_5$ and $Bi_{50}Sn_{40}Al_8Cu_2$ alloys in 0.5M HCl are listed in Table 4a. Corrosion rate of $Bi_{60}Sn_{40}$ alloy decreased after adding Sb-Zn or Sb-Ag but it increased after adding Al-Cd or Al-Cu. That is because adding Sb-Zn or Sb-Ag or Al-Cd or Al-Cu to $Bi_{60}Sn_{40}$ alloy caused microstructure changed and its affected microsegregation and reactivity of formed phases and other atoms with HCl solution. The $Bi_{50}Sn_{40}Sb_7Zn_3$ alloy has lowest corrosion current and corrosion rate values.

EFM is a non-destructive corrosion measurement technique. In which current responses due to a potential perturbation by one or more sine waves are measured at more frequencies than the frequency of the applied signal. The results of EFM experiments are a spectrum of current response as a function of frequency. The intermodulation spectrum of $Bi_{60}Sn_{40}$, $Bi_{50}Sn_{40}Sb_7Zn_3$, $Bi_{50}Sn_{40}Sb_7Ag_3$, $Bi_{50}Sn_{40}Al_5Cd_5$ and $Bi_{50}Sn_{40}Al_8Cu_2$ alloys in 0.5M HCl solution are shown in Figure 6. The larger peaks were used to calculate the corrosion current density (i_{corr}) and the corrosion rate and then listed in Table 4b. The corrosion current density (i_{corr}) of $Bi_{60}Sn_{40}$ alloy varied after adding alloying elements.

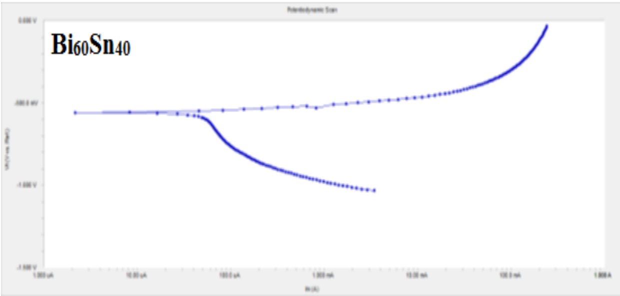

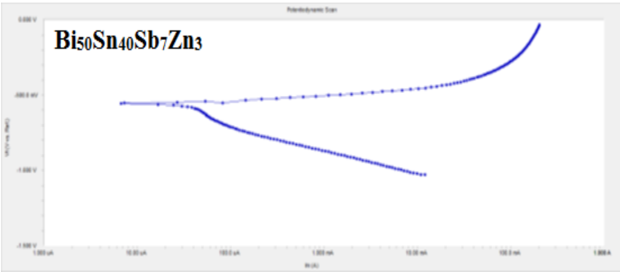

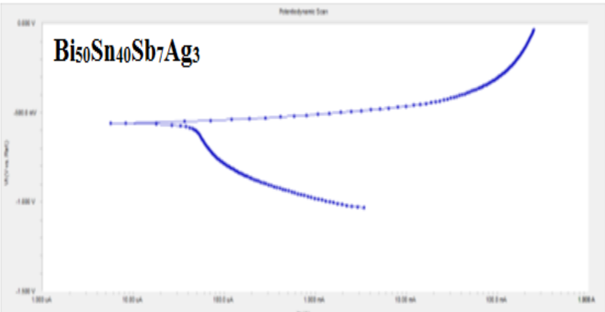

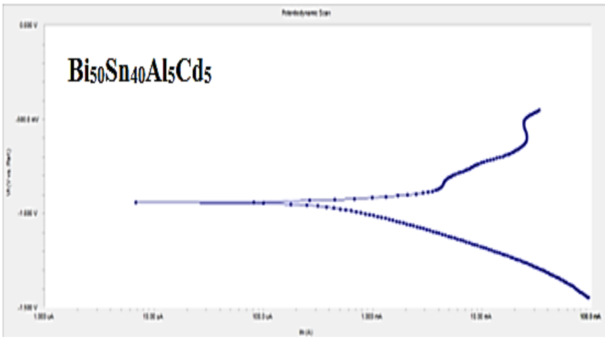

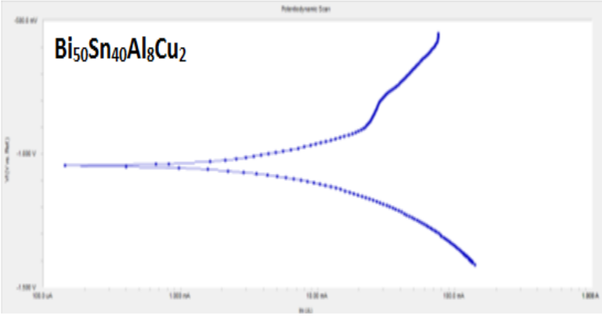

Figure 5:- electrochemical polarization curves of used alloys

Table 4a:- corrosion potential (E_{Corr}), corrosion current (I_{Corr}), and corrosion rate (C. R) of used alloys

Alloys	E mV	I_{Corr} µA	C. R mpy
$Bi_{60}Sn_{40}$	-557	36	49.01
$Bi_{50}Sn_{40}Sb_7Zn_3$	-437	2.24	3.05
$Bi_{50}Sn_{40}Sb_7Ag_3$	-558	28.1	38.26
$Bi_{50}Sn_{40}Al_5Cd_5$	-940	273	371
$Bi_{50}Sn_{40}Al_8Cu_2$	-1.04	321	4377

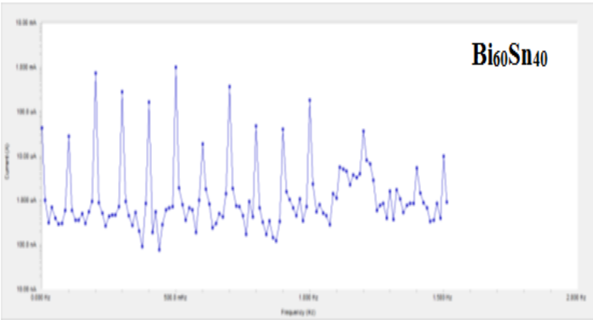

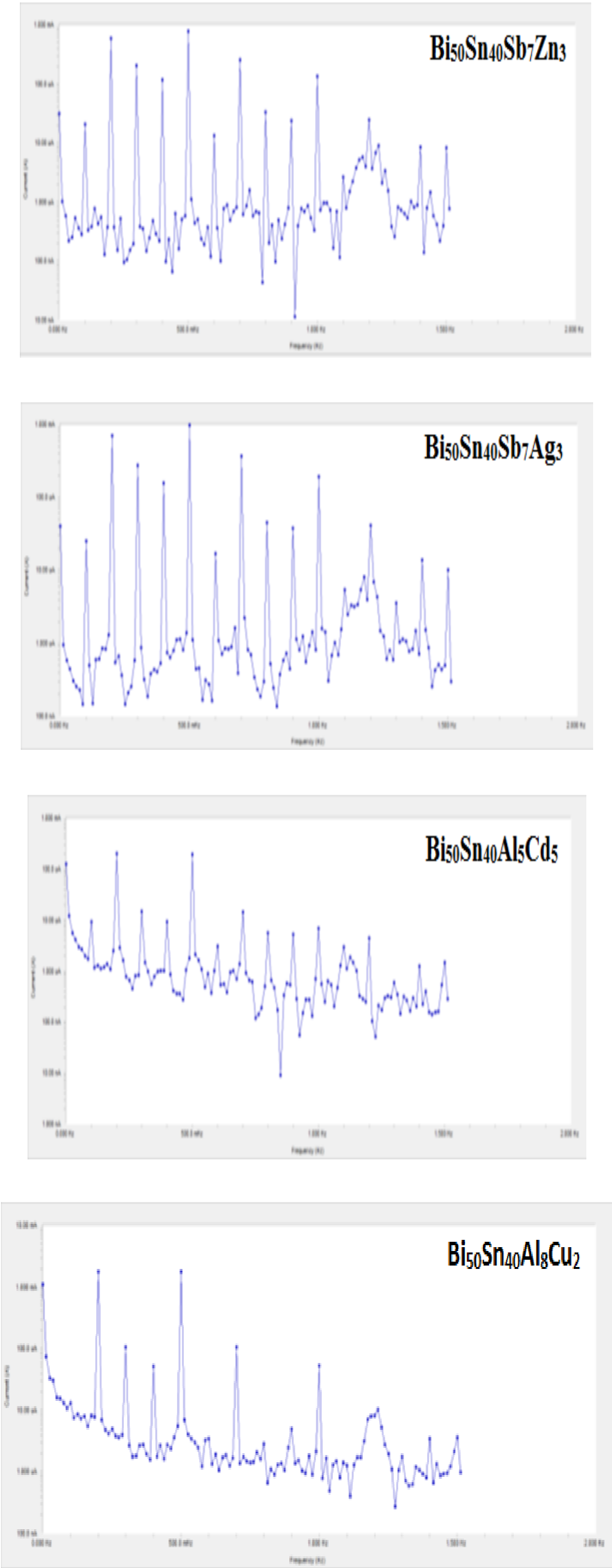

Figure 6:-intermodulation spectrum obtained by EFM technique for used alloys

Table 4a:- the corrosion current density (i_{corr}) and the corrosion rate (C. R) of used alloys

Alloys	i_{Corr} μa	C. R x 10^3 mpy
$Bi_{60}Sn_{40}$	1.202	1.638
$Bi_{50}Sn_{40}Sb_7Zn_3$	1.007	1.372
$Bi_{50}Sn_{40}Sb_7Ag_3$	1.086	1.480
$Bi_{50}Sn_{40}Al_5Cd_5$	1.347	1.836
$Bi_{50}Sn_{40}Al_8Cu_2$	14.79	20.16

IV. CONCLUSION

X-ray diffraction and scanning electron microscope analysis show that, the microstructure of $Bi_{60}Sn_{40}$ alloy changed after adding alloying elements. Contact angle of $Bi_{60}Sn_{40}$ alloy increased after adding Sb-Zn or Sb-Ag or Al-Cd or Al-Cu and a significant increased (28%) occurred after adding Al-Cd. The melting temperature of $Bi_{60}Sn_{40}$ alloy varied after adding alloying elements. The $Bi_{50}Sn_{40}Al_5Cd_5$ alloy has lowest melting temperature. Corrosion rate of $Bi_{60}Sn_{40}$ alloy decreased after adding Sb-Zn or Sb-Ag but it increased after adding Al-Cd or Al-Cu. The corrosion current density (i_{corr}) of $Bi_{60}Sn_{40}$ alloy varied after adding alloying elements.

V. REFERENCES

[1] M. Kamal, S. Mazen, A. B. El- Bediwi, E. Kashita, Radia. Eff. Def. Sol. 161 (2006) 143- 148

[2] A. B. El-Bediwi and M.M. El-Bahay, Radia. Eff. Def. Sol. 159 (2004) 133- 140

[3] M. Kamal, A. B. El- Bediwi, Radia. Eff. Def. Sol. 159 (2004) 6651

[4] A. B. El- Bediwi, E. Gouda, M. Kamal, A. M. S. E. Modeling C, 65:1 (2004)

[5] A. B. El-Bediwi, M.M. El-Bahay, M. Kamal, Radia. Eff. Def. Sol. 159 (2004) 491- 496

[6] M. Kamal, A. B. El-Bediwi and M. B. Karman, J. Mater. Sci.: Mater. Electro. 9 (1998) 425- 428

[7] M. Kamal, A. B. El-Bediwi, J. Mater. Sci.: Mater. Electro. 11 (2000) 519-523

[8] A. B. El-Bediwi, A. M. S. E. 75: 3 (2002) 1-12

[9] A. B. El-Bediwi, F. Dawood, M. Kamal, J. Advanc. Phys. 7:3 (2015) 1952

[10] A. B. El- Bediwi, F. Dawood, M. Kamal, Intern. J. Sci. Eng. . Appl. 4:2 (2015) 60- 63

[11] A. B. El- Bediwi, F. Dawood, M. Kamal, Intern. J. Curr. Res. 7: (2015) 16433

[12] Shepelevich, O.V. Gusakova and L.P. Shcherba chenko, Inorganic Mater. 1:49: 7 (2013) 663-667

[13] H. Chen, Z. Li, Z. Wu, Z. Zhang, J. Alloy. Compd. 394(2005) 282-285

[14] M. Kamal, S. Mazen, A. El-Bediwi, E. Kashita, Rad. Eff. Def. Sol. 161 (2006) 143

[15] E. Laine, I. Lähteenmākl, I. Lehtoranta, J. Mater. Sci., 13 (1978) 108

[16] M. Mc Cormack, H. S. Chen, G.W. Kammalott, S. Jin, J. Electron. Mater. 26: 8 (1997) 954

[17] W. Yoon and J.H. Perepezko, J. Mater. Sci., 33(1988)4300-4306

[18] G.L.F. Goldstein and J.W. Morris, J. Electro. Mater. 23: 5 (1994) 477-486

[19] B. D Cullity, "Element of x-ray diffraction" Ch.10 (1959) 297

[20] B. D. Cullity and S. R. Stock, Elements and x-ray diffraction, 3rd edn, (Prentice Hall). 2001

[21] C. Suryanarayana, Prog. Mater. Sci. 46: 1 (2001)